3D quantitative photoacoustic tomography using the δ-Eddington approximation

T. Saratoon[a], T. Tarvainen[b,c], S. R. Arridge[c] and B. T. Cox[a]

[a]Department of Medical Physics and Bioengineering, University College London, UK;
[b]Department of Applied Physics, University of Eastern Finland, Finland;
[c]Centre for Medical Image Computing and Department of Computer Science, University College London, UK

ABSTRACT

Quantitative photoacoustic tomography (QPAT) aims to recover the optical absorption and scattering properties of a tissue region from a given photoacoustic image. Since a photoacoustic image is proportional to the product of the absorption coefficient and the absorption-dependent light fluence, recovering these properties is a nonlinear, ill-posed inverse problem. The problem is typically large-scale, since we are generally interested in 3D images which possess high spatial resolution. It has previously been shown that a minimisation-based scheme can be used to succesfully recover the optical coefficients from 2D simulated photoacoustic images. This type of inversion seeks to adjust the desired model parameters until the difference between the measured and modelled data is minimised. Modelling a photoacoustic image requires a model of light transport in biological tissue, such as the radiative transfer equation (RTE) or the diffusion approximation (DA) to the RTE. The RTE is an accurate model of light transport, but its complexity means that it will require significant computational effort when solving such a large-scale problem using a minimisation-based inversion. The DA is a much more efficient model, however, since the DA breaks down at regions close to light sources it is not sufficiently accurate for QPAT. Here, we propose the use of the δ-Eddington approximation as a model of light transport for QPAT, which provides comparable computational efficiency as the DA whilst maintaining sufficient accuracy in regions close to sources. Details of the derivation of the δ-Eddington model and its incorporation into a gradient-based minimisation scheme are included, and the results of the inversion when using 2D and 3D simulated photoacoustic images are presented.

Keywords: Photoacoustic tomography, quantitative, chromophore concentrations, δ-Eddington approximation, gradient-based minimisation

1. QUANTITATIVE PHOTOACOUSTIC IMAGING

In photoacoustic tomography (PAT), an image is reconstructed from the measurements of the acoustic waves emitted following the absorption of a short pulse of laser light incident on a tissue region of interest. This image represents the distribution of initial pressure that arose following the absorption of optical energy, and is related, but not proportional, to the optical absorption coefficient of the tissue region. The aim of quantitative photoacoustic tomography (QPAT) is to determine the optical absorption coefficient from a given PAT image, and hence determine the related chromophore concentration distributions. Such a technique could be combined with a spectroscopic approach to provide functional information about the tissue, or used to obtain images of externally administered chromophores such as contrast agents, enabling molecular imaging.[1] However, since a PAT image is not directly proportional to the absorption coefficient, but is distorted by the light fluence, determining the absorption coefficient is nontrivial. This is because the fluence Φ depends on the absorption and scattering coefficients in the tissue (denoted μ_a and μ_s, respectively), so that the PAT image, which is an image of the initial pressure distribution p_0, is nonlinearly related to μ_a:

$$p_0(\boldsymbol{r}) = \Gamma(\boldsymbol{r})\mu_\mathrm{a}(\boldsymbol{r})\Phi(\boldsymbol{r};\mu_\mathrm{a}(\boldsymbol{r}),\mu_\mathrm{s}(\boldsymbol{r})), \qquad \boldsymbol{r}\in\Omega\in\mathbb{R}^3. \tag{1}$$

The Grüneisen parameter Γ is a thermodynamic property of the tissue, which we will assume is known throughout the domain Ω. This type of nonlinear, ill-posed inverse problem can be solved using a model-based minimisation

Photons Plus Ultrasound: Imaging and Sensing 2013, edited by Alexander A. Oraevsky, Lihong V. Wang,
Proc. of SPIE Vol. 8581, 85810V · © 2013 SPIE · CCC code: 1605-7422/13/$18 · doi: 10.1117/12.2004105

technique,[2–5] however, when choosing which model of light transport and which minimisation scheme to use it is important that we bear in mind the inherent large-scale of the problem. In PAT, we are generally interested in 3D images, and the spatial resolution will depend on the depth of the image. A typical image of size 1 cm^3 with a spatial resolution of 100 μm would possess 10^6 voxels, so that the inverse problem contains on the order of 10^6 unknowns. In Sec. 2 we discuss some possible choices of light model and motivate the use of the δ-Eddington approximation for 3D QPAT. In Sec. 3 we propose the use of a gradient-based minimisation scheme for 3D QPAT, and provide the relevant gradient calculations when using the δ-Eddington approximation in the forward PAT model. Results of the inversion using 2D and 3D simulated data are presented in Sec. 4 and discussed in Sec. 5.

2. MODELS OF LIGHT TRANSPORT

2.1 Radiative transfer equation

The radiative transfer equation (RTE) is an integro-differential equation which describes the transport of energy through an absorbing and scattering medium. The RTE is based on the principle of energy conservation, and balances the change in the radiance $\phi(\boldsymbol{r}, \hat{\boldsymbol{s}})$ at position $\boldsymbol{r}$ travelling in a direction of the unit vector $\hat{\boldsymbol{s}}$. The RTE, given by

$$(\hat{\boldsymbol{s}} \cdot \nabla + \mu_\text{a} + \mu_\text{s})\phi(\boldsymbol{r}, \hat{\boldsymbol{s}}) = \mu_\text{s} \int_{4\pi} \Theta(\hat{\boldsymbol{s}}, \hat{\boldsymbol{s}}')\phi(\boldsymbol{r}, \hat{\boldsymbol{s}}') \, \mathrm{d}\hat{\boldsymbol{s}}' + q, \tag{2}$$

where $\mu_\text{a} = \mu_\text{a}(\boldsymbol{r})$ and $\mu_\text{s} = \mu_\text{s}(\boldsymbol{r})$ are the absorption and scattering coefficients at position $\boldsymbol{r}$, respectively, and $\Theta(\hat{\boldsymbol{s}}, \hat{\boldsymbol{s}}')$ is the scattering phase function, describes how energy may be lost due to absorption and scattering out of the direction of interest, or may be gained through scattering into the direction of interest or from a source of energy $q = q(\boldsymbol{r}, \hat{\boldsymbol{s}})$. $\Theta(\hat{\boldsymbol{s}}, \hat{\boldsymbol{s}}')$ represents the fraction of light scattered from a direction $\hat{\boldsymbol{s}}'$ into a direction $\hat{\boldsymbol{s}}$, and is normalised such that

$$\int_{4\pi} \Theta(\hat{\boldsymbol{s}}, \hat{\boldsymbol{s}}') \, \mathrm{d}\hat{\boldsymbol{s}}' = 1. \tag{3}$$

Usually the form of Θ is not known, and since biological tissues have a complex structure, determining its form is nontrivial. The Henyey-Greenstein phase function,[6] which we will denote by Θ_HG, has been shown to accurately describe the scattering phase function in biological tissue.[7] The Henyey-Greenstein phase function can be written as an infinite sum of the Legendre polynomials P_n

$$\Theta_\text{HG} = \sum_{n=1}^{\infty} \frac{2n+1}{4\pi} g^n P_n(\hat{\boldsymbol{s}} \cdot \hat{\boldsymbol{s}}'), \tag{4}$$

where g is the average cosine of the phase function, given by

$$g = \int_{4\pi} \Theta(\hat{\boldsymbol{s}}, \hat{\boldsymbol{s}}')(\hat{\boldsymbol{s}} \cdot \hat{\boldsymbol{s}}') \, \mathrm{d}\hat{\boldsymbol{s}}, \tag{5}$$

and is often called the anisotropy factor since it describes the scattering anisotropy; $g = 0$ describes isotropic scattering, $0 < g \leq 1$ describes predominantly forward scattering and $-1 \leq g < 0$ describes predominantly backward scattering. Light scattering in biological tissue is generally forward concentrated, with typical anisotropy factors of $g \approx 0.9$.

The general solution to the RTE is not known, and analytic solutions are limited to simple conditions and geometries. Numerical solutions can be made to solve the RTE for more versatile conditions and arbitrary geometries, though since in PAT we are generally interested in 3D images, a numerical solution to the RTE will require significant computational memory and time due to the angular dependence of the phase function; the solution $\phi(\boldsymbol{r}, \hat{\boldsymbol{s}})$ is a function of angle at each point within the domain, so that the three-dimensional problem essentially becomes a four-dimensional problem. However, by making approximations to the scattering phase function the angular dependence can be removed entirely, resulting in a more tractable, albeit less accurate, model of light transport.

2.2 Diffusion approximation

The diffusion approximation (DA) to the RTE can be made by truncating the Henyey-Greenstein phase function (4) at $n = 1$.[8] This results in a new phase function, sometimes called the Eddington phase function, given by

$$\Theta_{\mathrm{E}} = \frac{1}{4\pi}(1 + 3g(\hat{\boldsymbol{s}} \cdot \hat{\boldsymbol{s}}')). \tag{6}$$

The radiance is also be written as a sum of Legendre polynomials, in which case the truncation at $n = 1$ means that the radiance can be expressed as

$$\phi(\boldsymbol{r}, \hat{\boldsymbol{s}}) = \frac{1}{4\pi}\Phi(\boldsymbol{r}) + \frac{3}{4\pi}\hat{\boldsymbol{s}} \cdot \boldsymbol{J}(\boldsymbol{r}), \tag{7}$$

where Φ is the fluence and $\boldsymbol{J}$ is the radiant flux vector, defined by

$$\Phi(\boldsymbol{r}) = \int_{4\pi} \phi(\boldsymbol{r}, \hat{\boldsymbol{s}}) \, \mathrm{d}\hat{\boldsymbol{s}}, \qquad \boldsymbol{J}(\boldsymbol{r}) = \int_{4\pi} \phi(\boldsymbol{r}, \hat{\boldsymbol{s}})\hat{\boldsymbol{s}} \, \mathrm{d}\hat{\boldsymbol{s}}. \tag{8}$$

The source term q is also written as a sum of Legendre polynomials. Using these approximations enable the derivation of a diffusion equation

$$(\mu_{\mathrm{a}} - \nabla \cdot \kappa(\boldsymbol{r})\nabla)\Phi(\boldsymbol{r}) = q_0(\boldsymbol{r}), \tag{9}$$

where κ is the diffusion coefficient, given by

$$\kappa = \frac{1}{3(\mu_{\mathrm{a}} + \mu_{\mathrm{s}}(1 - g))}, \tag{10}$$

and

$$q_0(\boldsymbol{r}) = \int_{4\pi} q(\boldsymbol{r}, \hat{\boldsymbol{s}}) \, \mathrm{d}\hat{\boldsymbol{s}}. \tag{11}$$

The removal of angular dependence means that the DA requires much less computational effort to solve than the RTE. However, the effect of using this approximation to the scattering phase function is that the scattering of light is assumed to be near-isotropic throughout the entire domain, though, as discussed in Sec. 2.1, the scattering of light in biological tissue is highly forward-peaked and will not behave diffusely until at least a few scattering events have occured. This move into the diffusive regime occurs around a few transport mean free paths away from the source, where a transport mean free path is given by $l = (\mu_{\mathrm{a}} + \mu_{\mathrm{s}}(1 - g))^{-1}$. For this reason, the DA breaks down at regions within a few transport mean free paths from any light sources, where the scattering of light in tissue cannot be considered diffuse. For PAT these regions are of great interest and may constitute a significant part of the image, and so the DA may not be a sufficiently accurate model of light transport for QPAT.

The expansion of the radiance and phase function into spherical harmonics is one of a number of ways to derive the DA,[8–10] and although the details have been omitted, the derivation of the diffusion equation above closely follows that of the delta-Eddington approximation below.

2.3 δ-Eddington approximation

The Eddington phase function approximation can be improved by incorporating an extra term, which has the effect of shifting a portion f of the light into the forward direction to better model the forward-peaked scattering of biological tissue. To obtain the δ-Eddington approximation, the phase function Θ_{E} is replaced by the delta-Eddington phase function $\Theta_{\delta\mathrm{E}}$ of Joseph *et al.*[11]

$$\Theta_{\delta-\mathrm{E}} = \frac{1}{4\pi}\left\{2f\delta(1 - (\hat{\boldsymbol{s}} \cdot \hat{\boldsymbol{s}}')) + (1 - f)(1 + 3\hat{g}(\hat{\boldsymbol{s}} \cdot \hat{\boldsymbol{s}}'))\right\}. \tag{12}$$

The modified anisotropy factor $\hat{g}$ can be found by considering that, in turbid media, the DA is valid at depths greater than a few transport mean free paths. In this region, the scattering of light is characterised solely by the

reduced scattering coefficient $\mu_s' = \mu_s(1-g)$. If we define the modified reduced scattering coefficient $\hat{\mu}_s' = \hat{\mu}_s(1-\hat{g})$ and enforce the requirement that this parameter remain unchanged, we can find an expression for the modified anisotropy factor $\hat{g}$:

$$\hat{\mu}_s' = \mu_s' \quad \Rightarrow \quad \mu_s(1-f)(1-\hat{g}) = \mu_s(1-g) \quad \Rightarrow \quad \hat{g} = \frac{g-f}{1-f}. \tag{13}$$

The parameter f can be chosen to best match an appropriate scattering phase function, for example, an empirical formula for calculating f as a function of g ($f = 0.026094g^3 + 0.023597g^2 + 0.13572g + 0.60366$) was determined by comparison with Monte Carlo simulations,[12] while comparison with the first n terms of the Henyey-Greenstein phase function results in a choice of $f = g^n$.

Given a suitable choice of f, the approximation to the phase function $\Theta \approx \Theta_{\delta-\mathrm{E}}$ can be substituted into the RTE (2) to give

$$(\hat{\boldsymbol{s}} \cdot \nabla + \mu_a + \hat{\mu}_s)\phi(\boldsymbol{r}, \hat{\boldsymbol{s}}) = \frac{\hat{\mu}_s}{4\pi} \int_{4\pi} (1 + 3\hat{g}(\hat{\boldsymbol{s}} \cdot \hat{\boldsymbol{s}}'))\phi(\boldsymbol{r}, \hat{\boldsymbol{s}}') \, \mathrm{d}\hat{\boldsymbol{s}}', \tag{14}$$

where $\hat{\mu}_s = (1-f)\mu_s$. The radiance may be separated into its collimated (ϕ_c) and scattered (ϕ_s) components

$$\phi(\boldsymbol{r}, \hat{\boldsymbol{s}}) = \phi_c(\boldsymbol{r}, \hat{\boldsymbol{s}}) + \phi_s(\boldsymbol{r}, \hat{\boldsymbol{s}}), \tag{15}$$

and hence the fluence can be separated similarly, since

$$\Phi(\boldsymbol{r}) = \int_{4\pi} \phi(\boldsymbol{r}, \hat{\boldsymbol{s}}) \, \mathrm{d}\hat{\boldsymbol{s}} = \int_{4\pi} \phi_c(\boldsymbol{r}, \hat{\boldsymbol{s}}) \, \mathrm{d}\hat{\boldsymbol{s}} + \int_{4\pi} \phi_s(\boldsymbol{r}, \hat{\boldsymbol{s}}) \, \mathrm{d}\hat{\boldsymbol{s}} = \Phi_c(\boldsymbol{r}) + \Phi_s(\boldsymbol{r}), \tag{16}$$

where Φ_c and Φ_s denote the collimated and scattered fluence, respectively. Substituting Eqs. (15) and (16) into Eq. (14) gives

$$(\hat{\boldsymbol{s}} \cdot \nabla + \mu_a + \hat{\mu}_s)(\phi_c(\boldsymbol{r}, \hat{\boldsymbol{s}}) + \phi_s(\boldsymbol{r}, \hat{\boldsymbol{s}})) = \frac{\hat{\mu}_s}{4\pi}(\Phi_c(\boldsymbol{r}) + \Phi_s(\boldsymbol{r})) + \frac{3\hat{g}\hat{\mu}_s}{4\pi} \int_{4\pi} (\hat{\boldsymbol{s}} \cdot \hat{\boldsymbol{s}}')(\phi_c(\boldsymbol{r}, \hat{\boldsymbol{s}}') + \phi_s(\boldsymbol{r}, \hat{\boldsymbol{s}}')) \, \mathrm{d}\hat{\boldsymbol{s}}'. \tag{17}$$

The collimated radiance includes both unscattered light and light scattered into the forward direction $\hat{\boldsymbol{z}}$, and is hence attenuated at a rate proportional to the transport coefficient $\hat{\mu}_t = \mu_a + \hat{\mu}_s$:

$$(\hat{\boldsymbol{s}} \cdot \nabla)\phi_c(\boldsymbol{r}, \hat{\boldsymbol{s}}) = -\hat{\mu}_t \phi_c(\boldsymbol{r}, \hat{\boldsymbol{s}}). \tag{18}$$

This can then be used to reduce Eq. (17) to

$$(\hat{\boldsymbol{s}} \cdot \nabla + \mu_a + \hat{\mu}_s)\phi_s(\boldsymbol{r}, \hat{\boldsymbol{s}}) = \frac{\hat{\mu}_s}{4\pi}(\Phi_c(\boldsymbol{r}) + \Phi_s(\boldsymbol{r})) + \frac{3\hat{g}\hat{\mu}_s}{4\pi} \int_{4\pi} (\hat{\boldsymbol{s}} \cdot \hat{\boldsymbol{s}}')(\phi_c(\boldsymbol{r}, \hat{\boldsymbol{s}}') + \phi_s(\boldsymbol{r}, \hat{\boldsymbol{s}}')) \, \mathrm{d}\hat{\boldsymbol{s}}'. \tag{19}$$

If the source is a monodirectional flux $I_0(\boldsymbol{r})$ incident in the positive z-direction, the solution to Eq. (18) is given by

$$\phi_c(\boldsymbol{r}, \hat{\boldsymbol{s}}) = I_0(\boldsymbol{r}) \exp\left(- \int_{z_0}^{z} \hat{\mu}_t(z') \, \mathrm{d}z' \right) \delta(1 - (\hat{\boldsymbol{s}} \cdot \hat{\boldsymbol{z}})), \tag{20}$$

where $\hat{\boldsymbol{z}}$ is a unit vector in the z-direction, which means the collimated fluence can be written as

$$\begin{aligned} \Phi_c(\boldsymbol{r}) &= \int_{4\pi} \phi_c(\boldsymbol{r}, \hat{\boldsymbol{s}}) \mathrm{d}\hat{\boldsymbol{s}} \\ &= I_0(\boldsymbol{r}) \exp\left(- \int_{z_0}^{z} \hat{\mu}_t(z') \, \mathrm{d}z' \right). \end{aligned} \tag{21}$$

Substituting Eqs. (20) and (21) into Eq. (19) then gives

$$(\hat{\boldsymbol{s}} \cdot \nabla + \mu_a + \hat{\mu}_s)\phi_s(\boldsymbol{r}, \hat{\boldsymbol{s}}) = \frac{\hat{\mu}_s}{4\pi}(\Phi_c(\boldsymbol{r}) + \Phi_s(\boldsymbol{r})) + \frac{3\hat{g}\hat{\mu}_s}{4\pi} \left\{ \Phi_c(\boldsymbol{r})(\hat{\boldsymbol{s}} \cdot \hat{\boldsymbol{z}}) + \int_{4\pi} (\hat{\boldsymbol{s}} \cdot \hat{\boldsymbol{s}}')\phi_s(\boldsymbol{r}, \hat{\boldsymbol{s}}') \, \mathrm{d}\hat{\boldsymbol{s}}' \right\}. \tag{22}$$

Analagous to Eq. (7) for the DA, the scattered radiance can be written as

$$\phi_{\mathrm{s}}(\boldsymbol{r},\hat{\boldsymbol{s}}) = \frac{1}{4\pi}\Phi_{\mathrm{s}}(\boldsymbol{r}) + \frac{3}{4\pi}(\hat{\boldsymbol{s}}\cdot\boldsymbol{J}_{\mathrm{s}}(\boldsymbol{r})), \tag{23}$$

where Φ_{s} is the scattered fluence and $\boldsymbol{J}_{\mathrm{s}}$ is the scattered radiant flux. This is substituted into Eq. (22) to give

$$\begin{aligned}(\hat{\boldsymbol{s}}\cdot\nabla)\Phi_{\mathrm{s}}(\boldsymbol{r}) &+ \mu_{\mathrm{a}}\Phi_{\mathrm{s}}(\boldsymbol{r}) + 3(\hat{\boldsymbol{s}}\cdot\nabla)(\hat{\boldsymbol{s}}\cdot\boldsymbol{J}_{\mathrm{s}}(\boldsymbol{r})) + 3(\mu_{\mathrm{a}}+\hat{\mu}_{\mathrm{s}})(\hat{\boldsymbol{s}}\cdot\boldsymbol{J}_{\mathrm{s}}(\boldsymbol{r}))\\ &= \hat{\mu}_{\mathrm{s}}(\Phi_{\mathrm{c}}(\boldsymbol{r})+\Phi_{\mathrm{s}}(\boldsymbol{r})) + \frac{3\hat{g}\hat{\mu}_{\mathrm{s}}}{4\pi}\left(\Phi_{\mathrm{s}}\int_{4\pi}(\hat{\boldsymbol{s}}\cdot\hat{\boldsymbol{s}}')\,\mathrm{d}\hat{\boldsymbol{s}}' + \int_{4\pi}(\hat{\boldsymbol{s}}\cdot\hat{\boldsymbol{s}}')(\boldsymbol{J}_{\mathrm{s}}(\boldsymbol{r})\cdot\hat{\boldsymbol{s}}')\,\mathrm{d}\hat{\boldsymbol{s}}'\right).\end{aligned} \tag{24}$$

Integrating Eq. (24) over all angles and using the solid angle vector integral identities

$$\int_{4\pi}\hat{\boldsymbol{s}}\cdot\mathbf{A}\,\mathrm{d}\hat{\boldsymbol{s}} = 0, \qquad \int_{4\pi}(\hat{\boldsymbol{s}}\cdot\mathbf{A})(\hat{\boldsymbol{s}}\cdot\mathbf{B})\,\mathrm{d}\hat{\boldsymbol{s}} = \frac{4\pi}{3}(\mathbf{A}\cdot\mathbf{B}), \tag{25}$$

which hold for arbitrary vectors $\mathbf{A}$ and $\mathbf{B}$, Eq. (24) reduces to an equation for the divergence of $\boldsymbol{J}_{\mathrm{s}}$:

$$\nabla\cdot\boldsymbol{J}_{\mathrm{s}}(\boldsymbol{r}) = \hat{\mu}_{\mathrm{s}}\Phi_{\mathrm{c}}(\boldsymbol{r}) - \mu_{\mathrm{a}}\Phi_{\mathrm{s}}(\boldsymbol{r}). \tag{26}$$

If instead we first multiply (24) by $\hat{\boldsymbol{s}}$ before integrating over all angles, and use the identities

$$\int_{4\pi}(\hat{\boldsymbol{s}}\cdot\mathbf{A})\hat{\boldsymbol{s}}\,\mathrm{d}\hat{\boldsymbol{s}} = \frac{4\pi}{3}\mathbf{A}, \qquad \int_{4\pi}(\hat{\boldsymbol{s}}\cdot\mathbf{A})(\hat{\boldsymbol{s}}\cdot\mathbf{B})\hat{\boldsymbol{s}}\,\mathrm{d}\hat{\boldsymbol{s}} = 0, \tag{27}$$

we find this reduces to

$$\frac{1}{3}\nabla\Phi_{\mathrm{s}}(\boldsymbol{r}) + (\mu_{\mathrm{a}}+\hat{\mu}_{\mathrm{s}}(1-\hat{g}))\boldsymbol{J}_{\mathrm{s}}(\boldsymbol{r}) = 3\hat{g}\hat{\mu}_{\mathrm{s}}\Phi_{\mathrm{c}}(\boldsymbol{r})\hat{\boldsymbol{z}}, \tag{28}$$

or equivalently,

$$\boldsymbol{J}_{\mathrm{s}}(\boldsymbol{r}) = 3\hat{g}\hat{\kappa}\hat{\mu}_{\mathrm{s}}\Phi_{\mathrm{c}}(\boldsymbol{r})\hat{\boldsymbol{z}} - \kappa\nabla\Phi_{\mathrm{s}}(\boldsymbol{r}), \tag{29}$$

where $\hat{\kappa}(\boldsymbol{r}) = (3(\mu_{\mathrm{a}}+\hat{\mu}_{\mathrm{s}}(1-\hat{g})))^{-1}$. Taking the divergence of Eq. (29) gives a second equation for the divergence of $\boldsymbol{J}_{\mathrm{s}}$:

$$\nabla\cdot\boldsymbol{J}_{\mathrm{s}}(\boldsymbol{r}) = -\nabla\cdot\hat{\kappa}\nabla\Phi_{\mathrm{s}}(\boldsymbol{r}) - 3\hat{g}\hat{\kappa}\hat{\mu}_{\mathrm{t}}\hat{\mu}_{\mathrm{s}}\Phi_{\mathrm{c}}(\boldsymbol{r}). \tag{30}$$

We can now equate Eqs. (26) and (30) to obtain a diffusion equation for the scattered fluence

$$(\nabla\cdot\kappa\nabla - \mu_{\mathrm{a}})\Phi_{\mathrm{s}}(\boldsymbol{r}) = -(1+3\hat{g}\hat{\kappa}\hat{\mu}_{\mathrm{t}})\hat{\mu}_{\mathrm{s}}\Phi_{\mathrm{c}}(\boldsymbol{r}), \tag{31}$$

where the right-hand side represents the collimated source. Thus, having found the collimated fluence Φ_{c} using Eq. (20), the scattered fluence Φ_{s} can be found by solving the diffusion equation (31) and the total fluence found using $\Phi = \Phi_{\mathrm{c}} + \Phi_{\mathrm{s}}$. The reduction to a diffusion equation means that the δ-Eddington approximation is comparitive to the DA in its computational efficiency, while the improved approximation to the scattering phase function improves the accuracy at regions close to the source.

3. MINIMISATION-BASED INVERSION

Generally in QPAT, the scattering coefficient μ_{s} will not be known in advance, and so it is necessary to recover both the absorption and scattering coefficients simultaneously from the measured PAT image. Model-based minimisation-based techniques, which seek to iteratively adjust the parameters in the model until the difference between the measured and modelled data is minimised, have previously been shown to succesfully recover the optical coefficients from 2D simulated PAT images.[2–5] Hessian- and Jacobian-based methods use the Hessian matrix of second partial derivatives, or an approximation to the Hessian made using the Jacobian matrix of first partial derivatives, to direct the minimisation. These methods can perform the inversion in relatively few iterations, though require significantly more memory than a gradient-based scheme.[13] In Sec. 1 we mentioned that the typical problem would contain around $N = 10^6$ unknowns. Since Hessian and Jacobian matrices have dimensions $N \times N$, storing these matrices would required on the order of terabytes of computer memory. Gradient-based methods, however, use only gradient information to approximate the Hessian matrix, and though they typically require a larger numer of iterations to perform the inversion, the gradient vector has dimensions $N \times 1$, requiring only megabytes of computer memory for a problem of the same size. For this reason, we choose to use a gradient-based minimisation scheme to perform the inversion for the optical coefficients μ_{a} and μ_{s}.

3.1 Functional gradient calculations

We will first assume that the Grüneisen parameter is known and constant, such that $\Gamma(\boldsymbol{r}) = 1 \; \forall \boldsymbol{r} \in \Omega$, so that $p_0 = \mu_\mathrm{a}\Phi = \mu_\mathrm{a}(\Phi_\mathrm{c} + \Phi_\mathrm{s})$. We seek a solution to

$$\underset{\mu_\mathrm{a},\mu_\mathrm{s}}{\operatorname{argmin}} \quad \varepsilon = \frac{1}{2}(p_0^{\mathrm{meas}} - p_0(\mu_\mathrm{a},\mu_\mathrm{s}))^\mathrm{T}(p_0^{\mathrm{meas}} - p_0(\mu_\mathrm{a},\mu_\mathrm{s})), \tag{32}$$

where p_0^{meas} and p_0 are the measured and modelled PAT images, respectively. To employ a gradient-based minimisation scheme, we will need to obtain an expression for the gradient of Eq. (32) with respect to $(\mu_\mathrm{a},\mu_\mathrm{s})$. This could be done using a finite difference method, whereby the absorption and scattering coefficients are perturbed at each point in the domain, and the resulting change in ε is noted. For our typical PAT image, such a method would require $2(N+2) = 2(10^6+2)$ runs of the forward model, and so a more efficient method for calculating the gradients is desirable.

The calculations which follow will be for the discrete case, whereby the diffusion model has been implemented using the finite element method (FEM), i.e. the diffusion equation for the scattered fluence (31) has been converted to its weak formulation and the domain is constructed from continuous piecewise linear basis functions $\psi_j(\boldsymbol{r})$, $j = 1,\ldots,N$, so that the scattered fluence can be written as

$$\Phi_\mathrm{s}(\boldsymbol{r}) \approx \Phi_\mathrm{s}^h(\boldsymbol{r}) = \sum_{i=1}^{N} \Phi_\mathrm{s}^i \psi^i(\boldsymbol{r}). \tag{33}$$

The absorption and scattering coefficients are also defined using a piecewise linear basis:

$$\mu_\mathrm{a}(\boldsymbol{r}) \approx \mu_\mathrm{a}^h(\boldsymbol{r}) = \sum_{i=1}^{N} \mu_\mathrm{a}^i \psi^i(\boldsymbol{r}), \quad \mu_\mathrm{s}(\boldsymbol{r}) \approx \mu_\mathrm{s}^h(\boldsymbol{r}) = \sum_{i=1}^{N} \mu_\mathrm{s}^i \psi^i(\boldsymbol{r}). \tag{34}$$

Having noted that these parameters are now expressed in this form, we will drop the superscript $(.)^h$ for notational convenience. More information on the numerical implementation of the diffusion equation using the FEM can be found in the literature.[14] Applying the FEM allows us to write Eq. (31) in the matrix form

$$A\Phi_\mathrm{s} = \mathbf{b}, \tag{35}$$

where, for $j = 1,\ldots,N$, $k = 1,\ldots,N$,

$$A_{jk} = \int_\Omega \hat{\kappa}(\boldsymbol{r}) \; \nabla\psi_k(\boldsymbol{r}) \cdot \nabla\psi_j(\boldsymbol{r}) \; \mathrm{d}\Omega + \int_\Omega \mu_\mathrm{a}(\boldsymbol{r}) \; \psi_k(\boldsymbol{r}) \cdot \psi_j(\boldsymbol{r}) \; \mathrm{d}\Omega \tag{36}$$

and

$$\mathbf{b} = (1 + 3\hat{g}\kappa\hat{\mu}_\mathrm{t})\hat{\mu}_\mathrm{s}\Phi_\mathrm{c}. \tag{37}$$

We now consider the functional gradient for the absorption coefficient μ_a. Differentiating Eq. (32) with respect to μ_a at a point $\boldsymbol{r}_i$ is given by

$$\frac{\partial\varepsilon}{\partial\mu_\mathrm{a}^i} = -\left(\frac{\partial p_0}{\partial\mu_\mathrm{a}^i}\right)^\mathrm{T}(p_0^{\mathrm{meas}} - p_0), \tag{38}$$

where $\mu_\mathrm{a}^i = \mu_\mathrm{a}(\boldsymbol{r}_i)$. The derivative of p_0 with respect to μ_a^i is given by

$$\frac{\partial p_0}{\partial\mu_\mathrm{a}^i} = \frac{\partial\mu_\mathrm{a}}{\partial\mu_\mathrm{a}^i}\Phi + \mu_\mathrm{a}\frac{\partial\Phi_\mathrm{c}}{\partial\mu_\mathrm{a}^i} + \mu_\mathrm{a}\frac{\partial\Phi_\mathrm{s}}{\partial\mu_\mathrm{a}^i}. \tag{39}$$

Substituting this into Eq. (38) and using the property of matrix transposes

$$(A_1A_2\ldots A_n)^\mathrm{T} = A_n^\mathrm{T}\ldots A_2^\mathrm{T}A_1^\mathrm{T}, \tag{40}$$

we find that

$$\frac{\partial \varepsilon}{\partial \mu_{\mathrm{a}}^i} = -\Phi^{\mathrm{T}} \left(\frac{\partial \mu_{\mathrm{a}}}{\partial \mu_{\mathrm{a}}^i} \right)^{\mathrm{T}} (p_0^{\mathrm{meas}} - p_0) - \left(\frac{\partial \Phi_{\mathrm{c}}}{\partial \mu_{\mathrm{a}}^i} \right)^{\mathrm{T}} \mu_{\mathrm{a}}^{\mathrm{T}} (p_0^{\mathrm{meas}} - p_0) - \left(\frac{\partial \Phi_{\mathrm{s}}}{\partial \mu_{\mathrm{a}}^i} \right)^{\mathrm{T}} \mu_{\mathrm{a}}^{\mathrm{T}} (p_0^{\mathrm{meas}} - p_0). \tag{41}$$

The first term can be calculated directly, and the second term requires differentiating Eq. (20) with respect to μ_{a}^i, which is simply the derivative of an exponentially decaying function. The third term requires the derivative of the scattered fluence, which we do not have a direct expression for. To obtain this, we differentiate Eq. (35) with respect to μ_{a}^i to obtain

$$\begin{aligned} \frac{\partial (A\Phi_{\mathrm{s}})}{\partial \mu_{\mathrm{a}}^i} &= \frac{\partial \mathbf{b}}{\partial \mu_{\mathrm{a}}^i} \\ \Rightarrow \frac{\partial A}{\partial \mu_{\mathrm{a}}^i}\Phi_{\mathrm{s}} + A\frac{\partial \Phi_{\mathrm{s}}}{\partial \mu_{\mathrm{a}}^i} &= \frac{\partial \mathbf{b}}{\partial \mu_{\mathrm{a}}^i} \\ \Rightarrow \frac{\partial \Phi_{\mathrm{s}}}{\partial \mu_{\mathrm{a}}^i} &= A^{-1}\left(\frac{\partial \mathbf{b}}{\partial \mu_{\mathrm{a}}^i} - \frac{\partial A}{\partial \mu_{\mathrm{a}}^i}\Phi_{\mathrm{s}} \right). \end{aligned} \tag{42}$$

Substituting this into (41) gives

$$\begin{aligned} \frac{\partial \varepsilon}{\partial \mu_{\mathrm{a}}^i} = &- \Phi^{\mathrm{T}} \left(\frac{\partial \mu_{\mathrm{a}}}{\partial \mu_{\mathrm{a}}^i} \right)^{\mathrm{T}} (p_0^{\mathrm{meas}} - p_0) - \left(\frac{\partial \Phi_{\mathrm{c}}}{\partial \mu_{\mathrm{a}}^i} \right)^{\mathrm{T}} \mu_{\mathrm{a}}^{\mathrm{T}} (p_0^{\mathrm{meas}} - p_0) \\ &- \left(\frac{\partial \mathbf{b}}{\partial \mu_{\mathrm{a}}^i} \right)^{\mathrm{T}} (A^{-1})^{\mathrm{T}} \mu_{\mathrm{a}}^{\mathrm{T}} (p_0^{\mathrm{meas}} - p_0) + \Phi_{\mathrm{s}}^{\mathrm{T}} \left(\frac{\partial A}{\partial \mu_{\mathrm{a}}^i} \right)^{\mathrm{T}} (A^{-1})^{\mathrm{T}} \mu_{\mathrm{a}}^{\mathrm{T}} (p_0^{\mathrm{meas}} - p_0), \end{aligned} \tag{43}$$

and, since $(A^{-1})^{\mathrm{T}} = (A^{\mathrm{T}})^{-1}$,

$$\begin{aligned} \frac{\partial \varepsilon}{\partial \mu_{\mathrm{a}}^i} = &- \Phi^{\mathrm{T}} \left(\frac{\partial \mu_{\mathrm{a}}}{\partial \mu_{\mathrm{a}}^i} \right)^{\mathrm{T}} (p_0^{\mathrm{meas}} - p_0) - \left(\frac{\partial \Phi_{\mathrm{c}}}{\partial \mu_{\mathrm{a}}^i} \right)^{\mathrm{T}} \mu_{\mathrm{a}}^{\mathrm{T}} (p_0^{\mathrm{meas}} - p_0) \\ &- \left(\frac{\partial \mathbf{b}}{\partial \mu_{\mathrm{a}}^i} \right)^{\mathrm{T}} (A^{\mathrm{T}})^{-1} \mu_{\mathrm{a}}^{\mathrm{T}} (p_0^{\mathrm{meas}} - p_0) + \Phi_{\mathrm{s}}^{\mathrm{T}} \left(\frac{\partial A}{\partial \mu_{\mathrm{a}}^i} \right)^{\mathrm{T}} (A^{\mathrm{T}})^{-1} \mu_{\mathrm{a}}^{\mathrm{T}} (p_0^{\mathrm{meas}} - p_0). \end{aligned} \tag{44}$$

We define the adjoint fluence Φ^* to be the solution to another diffusion equation

$$\begin{aligned} A^{\mathrm{T}}\Phi^* &:= \mu_{\mathrm{a}}^{\mathrm{T}} (p_0^{\mathrm{meas}} - p_0) \\ \Rightarrow \Phi^* &= (A^{\mathrm{T}})^{-1} \mu_{\mathrm{a}}^{\mathrm{T}} (p_0^{\mathrm{meas}} - p_0), \end{aligned} \tag{45}$$

and substitute this into Eq. (44) to obtain an expression for the absorption gradient:

$$\frac{\partial \varepsilon}{\partial \mu_{\mathrm{a}}^i} = -\Phi^{\mathrm{T}} \left(\frac{\partial \mu_{\mathrm{a}}}{\partial \mu_{\mathrm{a}}^i} \right)^{\mathrm{T}} (p_0^{\mathrm{meas}} - p_0) - \left(\frac{\partial \Phi_{\mathrm{c}}}{\partial \mu_{\mathrm{a}}^i} \right)^{\mathrm{T}} \mu_{\mathrm{a}}^{\mathrm{T}} (p_0^{\mathrm{meas}} - p_0) - \left(\frac{\partial \mathbf{b}}{\partial \mu_{\mathrm{a}}^i} \right)^{\mathrm{T}} \Phi^* + \Phi_{\mathrm{s}}^{\mathrm{T}} \left(\frac{\partial A}{\partial \mu_{\mathrm{a}}^i} \right)^{\mathrm{T}} \Phi^*. \tag{46}$$

The gradient for the scattering coefficient can be found analagously, and is given by

$$\frac{\partial \varepsilon}{\partial \mu_{\mathrm{s}}^i} = -\left(\frac{\partial \Phi_{\mathrm{c}}}{\partial \mu_{\mathrm{s}}^i} \right)^{\mathrm{T}} \mu_{\mathrm{a}}^{\mathrm{T}} (p_0^{\mathrm{meas}} - p_0) - \left(\frac{\partial \mathbf{b}}{\partial \mu_{\mathrm{s}}^i} \right)^{\mathrm{T}} \Phi^* + \Phi_{\mathrm{s}}^{\mathrm{T}} \left(\frac{\partial A}{\partial \mu_{\mathrm{s}}^i} \right)^{\mathrm{T}} \Phi^*. \tag{47}$$

The incorporation of the adjoint model means that both of these functional gradients can be calculated using only two runs of the forward model, rather than the $2(N+2)$ runs required of a finite difference calculation.

4. RESULTS

The gradient calculations described above were used in a gradient-based minimisation scheme, namely the limited-memory BFGS (l-BFGS) method[15] with a storage history of 15 iterations, to solve

$$\underset{\mu_{\mathrm{a}}, \mu_{\mathrm{s}}}{\operatorname{argmin}} \quad \varepsilon = \frac{1}{2} (p_0^{\mathrm{meas}} - p_0(\mu_{\mathrm{a}}, \mu_{\mathrm{s}}))^{\mathrm{T}} (p_0^{\mathrm{meas}} - p_0(\mu_{\mathrm{a}}, \mu_{\mathrm{s}})). \tag{48}$$

We include results for both 2D and 3D simulated photoacoustic data; in the 2D case we show the results when attempting to recover (μ_a, μ_s) simultaneously, and in the 3D case we show the results of recovering one coefficient when the other is known. In each case the measured data p_0^{meas} was simulated by defining some absorption and scattering coefficients (μ_a, μ_s) and solving the δ-Eddington approximation described in Sec. 2.3 for the fluence Φ. In the results which follow, we chose $f = g^2$ and $g = 0.9$, and the output flux $\boldsymbol{F}$ on the boundary $\partial\Omega$ when solving the diffusion equation for the scattered fluence Φ_s was given by

$$\boldsymbol{F}(\boldsymbol{r}_b) = -\,\hat{\kappa}(\boldsymbol{r}_b)\hat{\boldsymbol{n}}(\boldsymbol{r}_b)\cdot\nabla\Phi_s(\boldsymbol{r})|_{\partial\Omega(\boldsymbol{r}_b)}\,, \tag{49}$$

where $\boldsymbol{r}_b$ is a point on $\partial\Omega$ and $\hat{\boldsymbol{n}}$ is a unit vector normal to $\partial\Omega$. The true initial pressure distribution was then calculated from $p_0^{\text{true}} = \mu_a\Phi$, which was used an initial condition to solve the photoacoustic wave equation

$$\left(\frac{\partial^2}{\partial t^2} - c_s^2\nabla^2\right)p = 0, \tag{50}$$

whose initial conditions are given by

$$p(\boldsymbol{r},t)|_{t=0} = p_0^{\text{true}}(\boldsymbol{r}), \qquad \left.\frac{\partial p}{\partial t}\right|_{t=0} = 0, \tag{51}$$

where c_s is the sound speed and $p(\boldsymbol{r},t)$ represents the acoustic pressure at the point $\boldsymbol{r}$ and time t. The measured initial pressure distribution p_0^{meas}, which constitutes the measured data, was reconstructed from measurements of the acoustic pressure over some arbitrary measurement surface. Numerous image reconstruction algorithms for reconstructing the initial pressure distribution exist;[16] here, Eq. (50) was solved using a k-space, pseudo-spectral time domain model and a time-reversal reconstruction algorithm[17] was used to simulate a measured photoacoustic image p_0^{meas}. Since we are attempting to recover both absorption and scattering coefficients, this process was repeated for four different illumination positions to avoid the nonuniqueness problem.[18]

4.1 2D inversion results

To ensure that the optical coefficients were consistent with those typically found in biological tissue, the absorption coefficient μ_a and reduced scattering coefficient μ_s' were kept within a typical range of values: $\mu_a(\boldsymbol{r}) \in [0.01, 0.3]$ mm^{-1} and $\mu_s'(\boldsymbol{r}) \in [1, 3]$ mm^{-1} $\forall\boldsymbol{r} \in \Omega$, where Ω was an 8 mm $\times$ 8 mm square domain consisting of 6050 triangular mesh elements and 3136 nodal points. The absorption and scattering coefficients were defined on a piecewise linear nodal basis. To begin the minimisation, a starting value of $\mu_a = 0.01$ mm^{-1} and $\mu_s = 5$ mm^{-1} was used, i.e. the initial guess at (μ_a, μ_s) was their background values. Figs. 1(A) and 1(B) show the true absorption and scattering coefficients, respectively, and Figs. 1(C) and 1(D) show the recovered absorption and scattering coefficients, respectively, after 1000 iterations. Figs. 1(E) and 1(F) show profile comparisons of the true and recovered coefficients in the x-direction. The method was able to recover good estimates of both absorption and scattering coefficients, though the large number of iterations is mainly due to the slow convergence of the scattering coefficient. This can be seen in Fig. 2, which shows the percentage of the relative error in the absorption and scattering coefficient estimates, where the relative error ϵ is calculated using $\epsilon = (\mu_{a,s}^{\text{true}} - \mu_{a,s}^{\text{approx}})/\mu_{a,s}^{\text{true}}$. Although the absorption estimate does not improve much after around 250 iterations, the error does continue to decrease, albeit very slowly, indicating that the improvement in the scattering estimate does also improve the absorption estimate.

4.2 3D inversion results

The 3D simulations to provide measured data were performed on an $8 \times 8 \times 8$ mm domain with 29791 regular voxel elements and 32768 mesh nodes. The absorption and reduced scattering coefficients were kept within the range described in the 2D case to ensure that the optical coefficients were consistent with those found in biological tissue. Also consistent with the 2D inversions, the absorption and scattering coefficients were defined on a piecewise linear nodal basis, and the initial guess at (μ_a, μ_s) was chosen to be their background values.

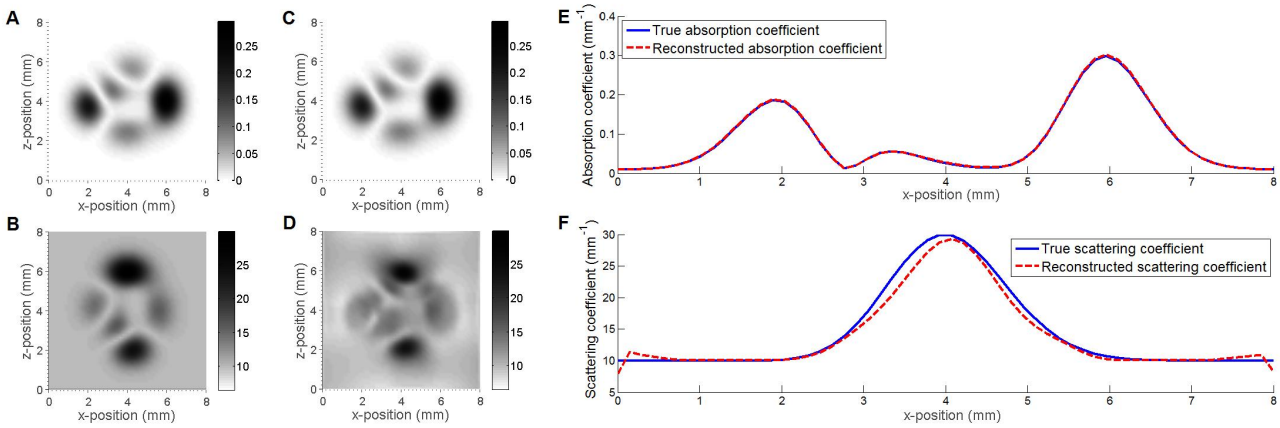

Figure 1. Inversion results using an l-BFGS minimisation scheme based on the δ-Eddington approximation and 2D simulated data after 1000 iterations. The method was used to recover both absorption and scattering coefficients simultaneously. Figs. A and B show the true absorption and scattering coefficients, respectively, in mm^{-1}. Figs. C and D show the recovered absorption and scattering coefficients using the same colorbar scale as Figs. A and B. Figs. E and F show a horizontal profile comparison of the true and recovered absorption and scattering coefficient, respectively.

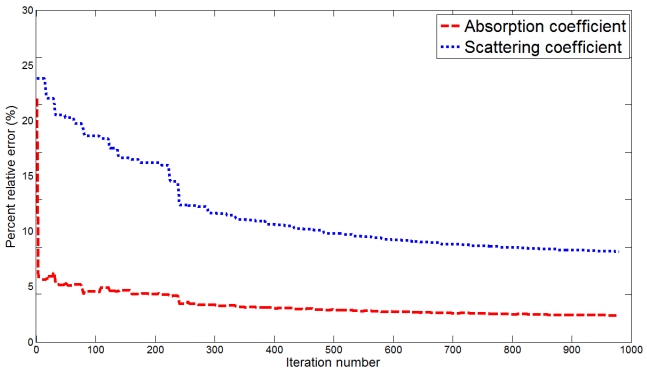

Figure 2. Percentage of the relative error in the absorption and scattering coefficients as the number of iterations of the gradient-based minimisation increases. The relative error ϵ is found using $\epsilon = (\mu_{\mathrm{a,s}}^{\mathrm{true}} - \mu_{\mathrm{a,s}}^{\mathrm{approx}})/\mu_{\mathrm{a,s}}^{\mathrm{true}}$.

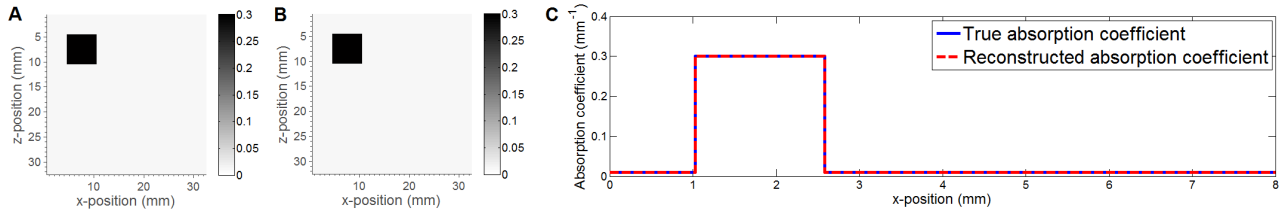

Figure 3. Inversion results using an l-BFGS minimisation scheme based on the δ-Eddington approximation and 3D simulated data after 10 iterations. The method was used to recover the absorption coefficient when the scattering coefficient is known. Fig. A shows a slice through the true absorption coefficient in mm^{-1}. Fig. B shows the same slice through the recovered absorption coefficient and uses the same colorbar scale as Fig. A. Fig. C shows a horizontal profile comparison of the true and recovered absorption coefficient.

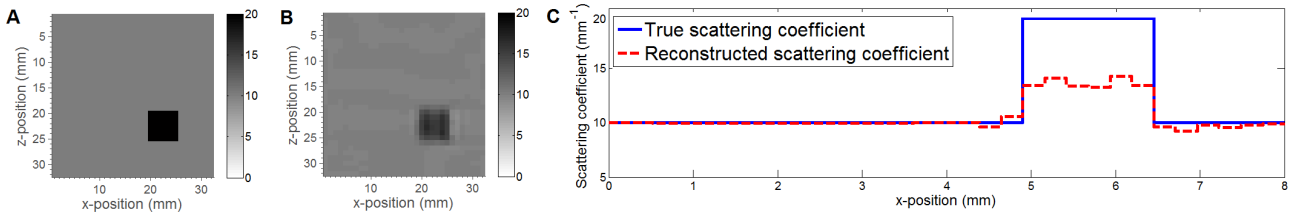

Figure 4. Inversion results using an l-BFGS minimisation scheme based on the δ-Eddington approximation and 3D simulated data after 200 iterations. The method was used to recover the scattering coefficient when the absorption coefficient is known. Fig. A shows a slice through the true scattering coefficient in mm^{-1}. Fig. B shows the same slice through the recovered scattering coefficient and uses the same colorbar scale as Fig. A. Fig. C shows a horizontal profile comparison of the true and recovered scattering coefficient.

4.2.1 Recover absorption: known scattering

For the 3D case, we first attempted to reconstruct the absorption coefficient when the scattering coefficient is known. In this case, we were able to recover the absorption coefficient almost exactly; Fig. 3(A) shows the true absorption coefficient and Fig. 3(B) shows the recovered absorption coefficient after 10 iterations. A horizontal profile comparison of the true and recovered absorption coefficient can be seen in 3(C).

4.2.2 Recover scattering: known absorption

Secondly, we attempted to reconstruct the scattering coefficient when the absorption coefficient is known. As seen in the 2D inversion, the scattering coefficient was much slower to converge to its true value than the absorption coefficient; Fig. 4(A) shows the true scattering coefficient and Fig. 4(B) shows the recovered scattering coefficient after 200 iterations. A horizontal profile comparison of the true and recovered scattering coefficient can be seen in 4(C).

5. DISCUSSION

This paper has investigated the use of the δ-Eddington approximation for 3D QPAT. The δ-Eddington approximation is more accurate than the DA in regions close to light sources, and is a significantly more efficient model of light transport than the 'gold-standard' RTE, making it a suitable choice for 3D minimisation-based inversions in QPAT. The δ-Eddington approximation was incorporated into our photoacoustic model, which was used in a gradient-based minimisation scheme, whereby the difference between the measured and modelled data was minimised with respect to the absorption and scattering coefficients. Inversions were performed using 2D and 3D simulated data, which included the simulation of acoustic propagation and reconstruction of the initial pressure distribution using a time-reversal method. In both cases we were able to recover good quantitative estimates of the absorption coefficient, however, the estimate of the scattering coefficient was much slower to converge to its true value. Similar difficulties in estimating the scattering coefficient have been seen in previous attempts at QPAT.[19]

The slow convergence of the scattering means that a large number of iterations will typically be required to obtain an accurate estimate of both optical coefficients simultaneously. In the 2D case this inversion may be quite manageable, however, PAT images are typically 3D and so the computational time required to perform 1000 iterations is significant enough that the method may be considered impractical. This problem, however, is not specific to the case when the δ-Eddington approximation is used to model PAT, but is an inherent property of the quantitative problem; the data $p_0^{\text{meas}} = \mu_{\text{a}}\Phi(\mu_{\text{a}}, \mu_{\text{s}})$ is much more weakly dependent on scattering than absorption. Considering this, the δ-Eddington approximation may still be considered the most practical model for this type of inversion scheme, since using e.g. the RTE to perform this number of iterations will require significantly more computational effort. The difficutly in recovering the scattering coefficient may not be a problem, however, depending on the required accuracy of the absorption coefficient: the scattering coefficient is not required to obtain chromophore concentrations, and the improvement in the absorption estimate is relatively small after a certain number of iterations. It may be sensible to consider the required accuracy of the resulting chromophore concentrations before attempting to recover both absorption and scattering coefficients. A sensible step forward might be to determine how well the absorption coefficient can be recovered if the scattering coefficient is fixed at some wrong value, say, the background value or mean value, and the effect that any error in this estimate has on the subsequent inversion for the desired chromophore concentrations.

ACKNOWLEDGMENTS

This work was supported by the Department of Medical Physics and Bioengineering at University College London, the Engineering and Physical Sciences Research Council, UK, the Academy of Finland (projects 136220, 140984, and 250215 Finnish Centre of Excellence in Inverse Problems Research) and by the strategic funding of the University of Eastern Finland. The authors would like to thanks Ossi Lehtikangas for his help with modelling collimated light sources using the RTE to validate the δ-Eddington light model.

REFERENCES

[1] Cox, B., Laufer, J. G., Arridge, S. R., and Beard, P. C., "Quantitative spectroscopic photoacoustic imaging: a review," *Journal of Biomedical Optics* **17**(6), 061202–1 (2012).

[2] Cox, B. T., Arridge, S. R., and Beard, P. C., "Gradient-based quantitative photoacoustic image reconstruction for molecular imaging," *Proceedings of SPIE* **6437**, 64371T–64371T–10 (2007).

[3] Cox, B., Tarvainen, T., and Arridge, S., "Multiple illumination quantitative photoacoustic tomography using transport and diffusion models," *Tomography and Inverse Transport Theory, American Mathematical Society, Contemporary Mathematics Series* **559**, 1–12 (2011).

[4] Gao, H., Zhao, H., and Osher, S., "Quantitative photoacoustic tomography," *UCLA CAM report* **11-28** (June 2011).

[5] Bal, G. and Ren, K., "On multi-spectral quantitative photoacoustic tomography in diffusive regime," *Inverse Problems* **28**(2), 025010 (2012).

[6] Henyey, L. and Greenstein, J., "Diffuse radiation in the galaxy," *Annales d'Astrophysique* **3**, 117 (1940).

[7] Jacques, S., Alter, C., and Prahl, S., "Angular dependence of HeNe laser light scattering by human dermis," *Lasers in the Life Sciences* **1**(4), 309–333 (1987).

[8] Arridge, S. R., "Optical tomography in medical imaging," *Inverse Problems* **41**, 40–93 (1999).

[9] Duderstadt, J. J. and Hamilton, L. J., [*Nuclear reactor analysis*], John Wiley and Sons, Inc., New York (1976).

[10] Ishimaru, A., [*Wave Propagation and Scattering in Random Media*], Academic Press Inc (1987).

[11] Joseph, J. and Wiscombe, W., "The delta-Eddington approximation for radiative flux transfer," *Journal of the Atmospheric Sciences* **33**, 2452–2459 (1976).

[12] Chai, C., Chen, Y., Li, P., and Luo, Q., "Improved steady-state diffusion approximation with an anisotropic point source and the delta-Eddington phase function," *Applied Optics* **46**(21), 4843–4851 (2007).

[13] Saratoon, T., Tarvainen, T., Cox, B., and Arridge, S., "A gradient-based method for quantitative photoacoustic tomography using the radiative transfer equation," *Inverse Problems, submitted* .

[14] Arridge, S., Schweiger, M., Hiraoka, M., and Delpy, D., "A finite element approach for modeling photon transport in tissue," *Medical Physics* **20**(2), 299–309 (1993).

[15] Nocedal, J. and Wright, S., [*Numerical Optimization*], Springer series in operations research, Springer, New York, NY, 2 ed. (2006).

[16] Kuchment, P. and Kunyansky, L., "Mathematics of Photoacoustic and Thermoacousic Tomography," in [*Handbook of Mathematical Methods in Imaging*], ch. 19, 817–865, Springer (2011).

[17] Treeby, B. E. and Cox, B. T., "k-Wave: MATLAB toolbox for the simulation and reconstruction of photoacoustic wave fields.," *Journal of Biomedical Optics* **15**(2), 021314 (2010).

[18] Bal, G. and Uhlmann, G., "Inverse diffusion theory of photoacoustics," *Inverse Problems* **26**, 085010 (Aug. 2010).

[19] Tarvainen, T., Cox, B. T., Kaipio, J. P., and Arridge, S. R., "Reconstructing absorption and scattering distributions in quantitative photoacoustic tomography," *Inverse Problems* **28**, 084009 (Aug. 2012).